Acta Crystallographica Section D
Biological Crystallography
ISSN 1399-0047

Perdeuteration: improved visualization of solvent structure in neutron macromolecular crystallography

S. J. Fisher,[a,b]‡ M. P. Blakeley,[a] E. I. Howard,[c] I. Petit-Haertlein,[a] M. Haertlein,[a] A. Mitschler,[d] A. Cousido-Siah,[d] A. G. Salvay,[c,e] A. Popov,[f] C. Muller-Dieckmann,[f] T. Petrova[g] and A. Podjarny[d]*

[a]Institut Laue–Langevin, 71 Avenue des Martyrs, 38000 Grenoble, France, [b]Department of Molecular Biology, University of Salzburg, 11 Billrothstrasse, 5020 Salzburg, Austria, [c]IFLYSIB, UNLP–CONICET, Calle 59, 789, B1900BTE La Plata, Argentina, [d]Department of Integrative Biology, IGBMC, CNRS, INSERM, Université de Strasbourg, 1 Rue Laurent Fries, Illkirch, France, [e]Universidad Nacional de Quilmes, Roque Saenz Pena 352, B1876BXD Bernal, Argentina, [f]ESRF, 6 Rue Jules Horowitz, 38043 Grenoble, France, and [g]Institute of Mathematical Problems of Biology, Russian Academy of Sciences, Pushchino 142290, Russian Federation

‡ Current address: Diamond Light Source, Didcot, Oxfordshire OX11 0DE, England.

Correspondence e-mail: apodjarny@gmail.com

© 2014 International Union of Crystallography

Received 17 July 2014
Accepted 30 September 2014

PDB reference: neutron structure of leucine and valine methyl-protonated type III antifreeze, 4ny6

The 1.8 Å resolution neutron structure of deuterated type III antifreeze protein in which the methyl groups of leucine and valine residues are selectively protonated is presented. Comparison between this and the 1.85 Å resolution neutron structure of perdeuterated type III antifreeze protein indicates that perdeuteration improves the visibility of solvent molecules located in close vicinity to hydrophobic residues, as cancellation effects between H atoms of the methyl groups and nearby heavy-water molecules (D_2O) are avoided.

1. Introduction

In neutron macromolecular crystallography, the replacement of hydrogen (H) by its isotope deuterium (D) is advantageous for two main reasons. Firstly, hydrogen has an anomalously large incoherent scattering cross-section, while that of deuterium is ∼40 times lower (Table 1). Since H atoms constitute around half of the atoms in a macromolecular crystal, their incoherent scattering signal contributes significantly to a high scattered background; H/D isotopic replacement therefore enhances the signal-to-noise ratio of the diffraction data by lowering the incoherent background. This allows weaker high-resolution reflections to be better resolved, thereby extending the resolution limit.

Secondly, as the coherent scattering length of deuterium (+6.67 fm) is positive and approximately twice that of hydrogen (−3.74 fm), D atoms are more readily located in neutron maps than H atoms. Neutron studies are most commonly performed using single crystals pre-soaked in D_2O solutions (Tomanicek *et al.*, 2010; Kovalevsky *et al.*, 2011; Fisher *et al.*, 2012; Yokoyama *et al.*, 2013; Oksanen *et al.*, 2014; Casadei *et al.*, 2014). Soaking allows the exchange of solvent-accessible H atoms attached to O or N atoms, but not those H atoms attached to C atoms. Since these represent ∼80–85% of all H atoms, a considerable incoherent signal still remains and thus large crystal volumes (typically >1 mm^3) are required for high-resolution data collection. Neutron data collected from D_2O-soaked crystals allows D atoms attached to O or N atoms to be readily visualized (at ≤2.5 Å resolution); however, at the resolutions typically attained (2–2.5 Å) for neutron protein crystallographic studies (Blakeley, 2009) cancellation effects (between positive and negative neutron scatterers) often limit the visualization of H atoms attached to aliphatic C atoms (*e.g.* CH_2 and CH_3 groups). In order to readily locate H atoms within neutron maps, data must extend to ∼1.5 Å resolution or better (Ostermann *et al.*, 2002; Kurihara *et al.*, 2004; Chen *et al.*, 2012). Historically, data sets were of relatively low completeness (by X-ray standards) and thus the resulting

Table 1
Neutron coherent scattering lengths and incoherent cross-sections for the common elements of a macromolecule.

Isotope	Atomic No.	Neutron coherent scattering length (fm)	Neutron incoherent cross-section (barns)†
^{1}H	1	−3.74	80.27
^{2}H (D)	1	6.67	2.05
^{12}C	6	6.65	0.00
^{14}N	7	9.37	0.50
^{16}O	8	5.81	0.00
^{31}P	15	5.13	0.01
^{32}S	16	2.80	0.00

† 1 barn = 10^{-28} m^2.

maps could be difficult to interpret; more recently, a concerted effort to achieve higher completeness has been made by, for example, collecting data from multiple crystal orientations. Studies have also been performed using perdeuterated crystals produced *via* bacterial expression on deuterated media (Hazemann *et al.*, 2005; Petit-Haertlein *et al.*, 2009). As perdeuteration provides complete deuteration of the protein, this leads to vastly improved signal-to-noise ratios and enables data to be collected in shorter times (Munshi *et al.*, 2012), to higher resolution (Cuypers *et al.*, 2013) and from smaller (∼0.1 mm^3) crystal volumes (Blakeley *et al.*, 2008; Howard *et al.*, 2011; Weber *et al.*, 2013), a critical advance that makes larger unit-cell systems more accessible to study. Moreover, cancellation effects are avoided with perdeuteration, allowing all D atoms to be readily visualized (at ≤2.5 Å resolution), including those attached to aliphatic C atoms (*e.g.* CD_2 and CD_3 groups). Many of the advantages of perdeuteration have been demonstrated by our recent neutron crystallographic study of type III antifreeze protein (Howard *et al.*, 2011).

Antifreeze proteins (AFP) allow certain organisms to survive in subzero environments by binding, through an 'ice-binding surface' (IBS), to ice-crystal nuclei as they form, inhibiting their further growth. The neutron structure was determined to 1.85 Å resolution (PDB entry 3qf6; Howard *et al.*, 2011) using a perdeuterated crystal of only 0.13 mm^3. The neutron diffraction data revealed a tetrahedral 'ice-like' cluster of four water molecules at the IBS that was not observed in previous X-ray studies; using these waters, it was possible to model the AFP–ice interaction and to illustrate that the hydrophobic residues of the IBS bind to, and recognize ice, *via* the holes in the six-membered rings of the ice crystal structure. In the course of parallel work for methodological purposes (Petit-Haertlein *et al.*, 2010; Weiss *et al.*, 2008), we also produced a deuterated type III AFP in which the methyl groups of leucine and valine residues are selectively protonated, *i.e.* the protein is identical to the perdeuterated protein except that CD_3 groups of leucine and valine residues are replaced by CH_3 groups. Having collected quasi-Laue neutron diffraction data from a crystal of the selectively protonated deuterated type III AFP, we here report a comparison between the resulting 1.8 Å resolution structure and the 1.85 Å resolution structure of perdeuterated type III AFP. In particular, these samples provide an opportunity to analyse the effect of the negative scattering signal of methyl H atoms, not only on the C atom to which they are bound but also on neighbouring heavy-water molecules (*i.e.* D_2O).

2. Materials and methods

2.1. Expression, purification and crystallization

Selectively protonated deuterated type III AFP was expressed, purified and crystallized as described previously (Petit-Haertlein *et al.*, 2010). Crystals were grown using the sitting-drop vapour-diffusion method at 285 K. A 50 µl drop consisting of 20 µl protein solution (10 mg ml^{-1}) and 30 µl reservoir solution was equilibrated against a 1 ml reservoir consisting of 2.1 *M* ammonium sulfate and 9% glycerol-d_8. A seed crystal obtained in one drop was then washed and placed into a new pre-equilibrated 48 µl sitting drop. This crystal grew to final dimensions of 1.60 × 0.38 × 0.38 mm (a volume of 0.23 mm^3).

2.2. Data collection

Neutron quasi-Laue diffraction data were collected from selectively protonated deuterated type III AFP crystals at 293 K on the LADI-III instrument (Blakeley *et al.*, 2010) at the Institut Laue–Langevin and extended to 1.80 Å resolution. As is typical for a quasi-Laue experiment, the crystal was held stationary at different φ angles. 13 images were collected spaced $\Delta\varphi = 7^\circ$ apart with an exposure time of 24 h, followed by a low-resolution pass using an exposure time of 2 h. The crystal orientation was then modified and both passes were repeated. The final data set consisted of 60 images with an average exposure time of 11.8 h. These were indexed and integrated using *LAUEGEN* (Campbell *et al.*, 1998) and the resulting data were wavelength-normalized using *LSCALE* (Arzt *et al.*, 1999). The data were then scaled and merged using the *CCP*4 program *SCALA* (Winn *et al.*, 2011). Data-collection and processing statistics for the neutron data can be found in Table 2. Advances in sample-environment options now allow the routine collection of neutron data at cryo-temperatures (Coates *et al.*, 2014), which not only can improve the nuclear scattering density definition for mobile side chains and water molecules (Blakeley *et al.*, 2004) but also allows the study of cryo-trapped intermediates (Casadei *et al.*, 2014).

2.3. Structure refinement

The previously deposited perdeuterated neutron structure of type III AFP (PDB entry 3qf6) was used as the starting model and the corresponding X-ray diffraction data (at 1.05 Å resolution, measured at ID29, ESRF; de Sanctis *et al.*, 2012) were used for the joint X-ray/neutron refinement of the selectively protonated deuterated type III AFP. The assumption here is that the X-ray data from the selectively protonated deuterated crystals should be the same as those from the perdeuterated crystal, as H and D are equivalent using X-rays. To obtain an initial refinement model, the original model was randomly perturbed and multiple conformations and all water molecules were removed. Restrained joint X-ray and neutron (Afonine *et al.*, 2010) refinement was then conducted using

Table 2
Neutron data-collection and processing statistics for selectively protonated deuterated type III antifreeze protein.

Values in parentheses are for the highest resolution shell.

Neutron source/instrument	ILL, LADI-III
Space group	$P2_12_12_1$
Unit-cell parameters	
a (Å)	32.7
b (Å)	39.1
c (Å)	46.5
α (°)	90
β (°)	90
γ (°)	90
Wavelength (Å)	3.25–4.10
No. of images	60
Angle between images (°)	7
Average exposure time (min)	710
Resolution (Å)	46.52–1.80 (1.90–1.80)
Total reflections	57643 (2085)
Unique reflections	5194 (591)
Completeness (%)	89.3 (71.4)
Multiplicity	11.1 (3.5)
$\langle I/\sigma(I)\rangle$	14.0 (6.6)
$R_{\rm merge}$	0.136 (0.169)
$R_{\rm p.i.m}$	0.035 (0.085)

the *PHENIX* suite (Adams *et al.*, 2010). D_2O molecules were added according to clear positive peaks in the $F_o - F_c$ difference nuclear scattering density maps. Occasionally, the X-ray and neutron positions of water molecules differ slightly; therefore, once added the positions of these molecules were fixed in order to stop the X-ray data biasing the refinement. 42 water molecules were added, with 39 modelled as full D_2O molecules. A further three were partially disordered, showing spherical density, and were modelled as O atoms only. For the atomic displacement parameters (ADPs) an anisotropic model was used for heavy atoms (*i.e.* C, N, O and S) and an isotropic model was used for H/D atoms, thus resulting in lower ADPs than is usual for neutron data refined alone. D atoms were added with the program *ReadySet!* (Adams *et al.*, 2010). Multiple conformations were modelled for Gln9, Val20, Glu25, Thr28, Pro33, Pro38, Asp36, Met43, Val45 and Leu55. All model modifications were made with the modelling program *Coot* (Emsley & Cowtan, 2004). The final model

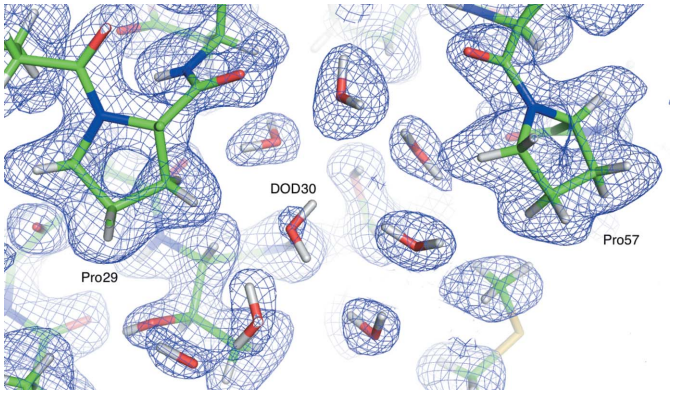

Figure 1
Water cluster positioned between Pro29 and Pro57. The $2F_o - F_c$ nuclear scattering density map is shown in blue (contoured at 1.5 r.m.s.). The orientation of DOD30 is visible at a lower σ level of 1.0 r.m.s..

Table 3
Model-refinement statistics for perdeuterated type III antifreeze protein (X-ray data) and selectively protonated deuterated type III antifreeze protein (neutron data).

Ramachandran criteria are as defined by *MolProbity* (Chen *et al.*, 2010).

	X-ray (perdeuterated type III AFP)	Neutron (selectively protonated deuterated type III AFP)
PDB code	4ny6	
Resolution (Å)	18.97–1.05	26.77–1.85
R (%)	17.0	17.6
$R_{\rm free}$ (%)	18.8	22.5
No. of reflections	28511	4897
R.m.s.d.		
Bonds (Å)	0.013	
Angles (°)	1.253	
No. of atoms	1256	
No. of D atoms	552	
No of H atoms	114	
No. of solvent molecules	42 (39 D_2O, 3 O)	
B factor (Å^2)		
All atoms	19.1	
Protein	17.9	
Solvent	31.7	
Ramachandran plot (%)		
Favoured	98.7	
Additional	1.3	
Outliers	0.0	

resulted in a neutron R factor of 17.6% and $R_{\rm free}$ of 22.5% and an X-ray R factor of 17.0% and $R_{\rm free}$ of 18.8%. Refinement statistics can be found in Table 3.

3. Discussion

The neutron diffraction data for the selectively protonated deuterated structure are of excellent quality, resulting in very clear nuclear scattering density maps. As an example, Fig. 1 shows a cluster of eight heavy-water molecules between Pro29 and Pro57, with 'boomerang'-shaped density indicating their orientations.

The D atoms visible in the nuclear scattering density maps add important structural information. For example, the orientation of an asparagine residue can be difficult to establish based solely on X-ray diffraction data (unless very high-resolution data are available) owing to the similar scattering lengths for oxygen and nitrogen. With neutrons, however, the D atoms of the carboxamide group are clearly visible and allow the correct orientation to be established (Fig. 2*a*). Similarly, the orientations of the methyl groups of residues such as isoleucine and the hydroxyl groups of residues such as tyrosine are clearly visible in the nuclear scattering density maps (Figs. 2*b* and 2*c*).

The selectively protonated residues (valine and leucine) are easily identifiable in the resulting nuclear scattering density maps. Fig. 3(*a*) shows Leu10 with a characteristic reduction in scattering density around the associated C atoms owing to the methyl H atoms cancelling with the C atoms. Looking at an OMIT map (Bhat, 1988; Fig. 3*b*, in which the H atoms were removed from the PDB file and another round of refinement was conducted), the resulting difference nuclear scattering

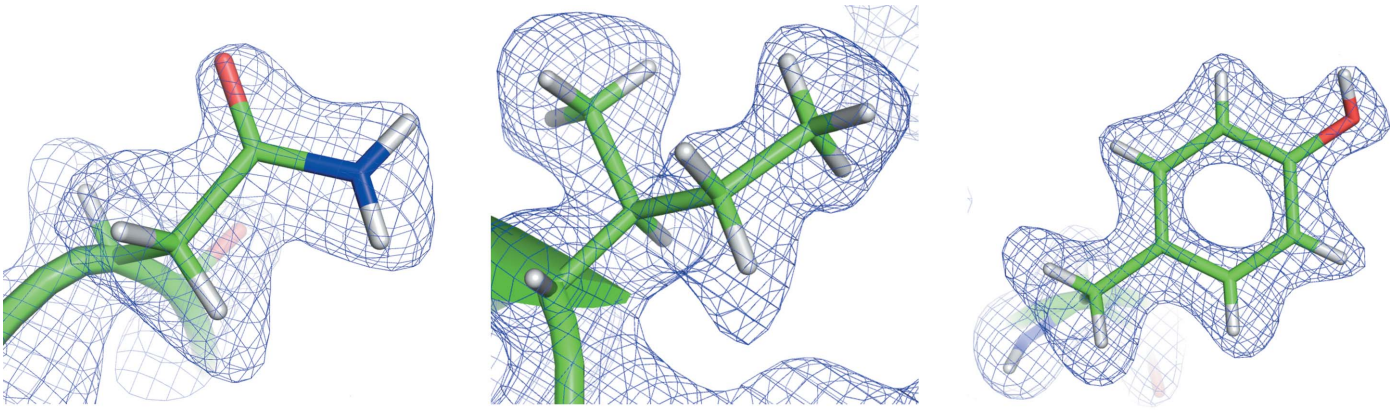

Figure 2
Examples of residues for which neutron diffraction data can assist in correctly positioning the side-chain atoms: (*a*) Asn8, (*b*) Ile37 and (*c*) Tyr63. Nuclear scattering density maps are shown in blue (contoured at 1.3 r.m.s.).

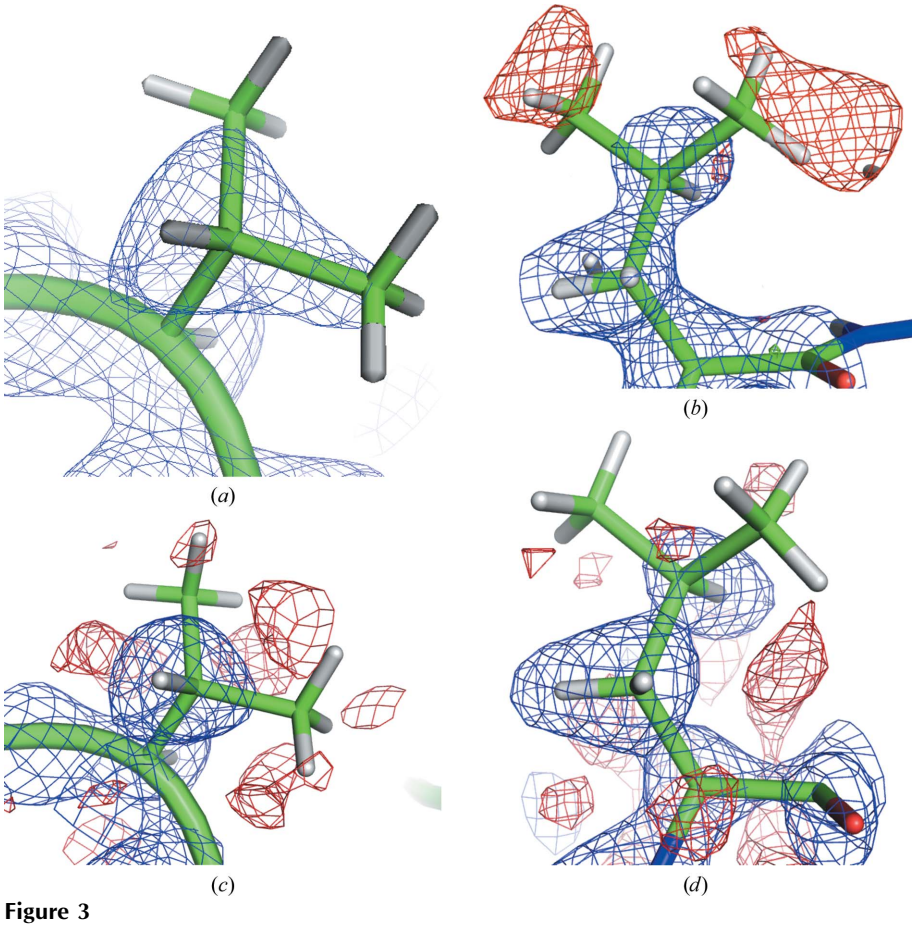

Figure 3
(*a*) $2F_o - F_c$ map for Val6 (shown in blue contoured at 1.5 r.m.s.). (*b*) $F_o - F_c$ OMIT map (in which the H atoms were omitted) for methyl-protonated Leu10 (shown in red contoured at -2.5σ). (*c*, *d*) Calculated F_c maps at 1.5 r.m.s. (blue) and -1.5 r.m.s. (red) for (*c*) Val6 and (*d*) Leu10.

density map shows negative peaks for the methyl H atoms. However, owing to the resolution limit these peaks are not individual H atoms as such, but rather show some smearing. Figs. 3(*c*) and 3(*d*) show calculated nuclear scattering density maps for Val6 and Leu10; these also indicate that individual H atoms would not be visible at the resolution limit of the data. Furthermore, given the rotational freedom of the CH_3 group the resulting nuclear scattering density maps are an average of the different positions.

3.1. Comparison of the neutron structures of selectively protonated deuterated type III antifreeze protein and perdeuterated type III antifreeze protein

The perdeuterated neutron structure and the selectively protonated deuterated neutron structure are very similar, with root-mean-square deviations of 0.10 Å on C^{α} atoms and of 0.46 Å on all atoms. The differences arise mainly owing to multiple conformations, of which there are three more in the selectively protonated deuterated structure (Pro33, Met43 and Val45).

Comparing the main-chain average *B* factors between the two structures (Fig. 4) indicates that the *B* values are slightly higher (on average 5.1 $Å^2$ larger) in the selectively protonated deuterated neutron structure, but the areas of high and low *B* values correspond in the two structures. We suggest that the difference in *B* values may be accounted for by the shift in the Wilson *B* factor between the two structures. In the perdeuterated structure this is 5.3 $Å^2$ and in the selectively hydrogenated structure it is 12.9 $Å^2$.

Despite the two neutron diffraction data sets (selectively protonated deuterated *versus* perdeuterated) being at equivalent temperatures, similar resolutions and levels of completeness, the overall solvent structures are rather different, with 42 water molecules in the selectively proto-

nated deuterated structure compared with 70 in the perdeuterated neutron structure. As 16 of the 65 amino-acid residues (∼25%) in each monomer are valine or leucine residues, in the selectively protonated deuterated structure the H atoms of the methyl groups of these valine and leucine residues scatter neutrons negatively and thus may cause cancellation not only of the nuclear scattering density of the C atom to which they are bound, but also of positive nuclear scattering density corresponding to heavy-water (D_2O) molecules in close vicinity. Comparing the individual water-molecule sites between the two structures indicates that 32 of the 42 are in equivalent positions, with another three in nearby positions. Of those in the same positions, 15 have the same orientation. Fig. 5 shows a comparison of the *B* factors for the water molecules in the two structures.

The perdeuterated structure shows 13 water molecules facing the IBS. Six of these are seen in the selectively protonated deuterated structure, of which four are in the same orientation. The *B* factors of these water molecules are comparable between the two neutron structures, with the perdeuterated structure having slightly lower values overall. Interestingly, despite the large number of hydrophobic residues on the IBS, the overall *B* factors for water molecules in this area do not seem to be particularly elevated compared with the water molecules bound elsewhere in the structure. Therefore, the reduction in the number of water molecules observed does not appear to be related to the *B* factors. It could be linked to density-cancellation effects caused by the three (out of a total of 12) selectively protonated residues of the IBS. Fig. 6 shows a comparison of the water molecules between the selectively protonated deuterated neutron structure and the perdeuterated neutron structure. The three highlighted regions show where there are significantly fewer solvent molecules in the selectively protonated deuterated structure compared with the perdeuterated structure. In all three of these cases the regions are in close proximity to a selectively protonated residue (Val20, Val26 and Val30).

Of the 13 water molecules identified at the IBS in the perdeuterated structure, four of them form a tetrahedral water cluster, which was critical in explaining the type III AFP ice-binding mechanism. In the selectively protonated deuterated neutron structure only two of these four tetrahedral water molecules are visible. Contouring to a lower σ level (1.5σ) in the $F_o - F_c$ difference map shows a small peak around 1 Å from one of the missing water molecules; however, this is not discernable from the surrounding noise. This is perhaps owing

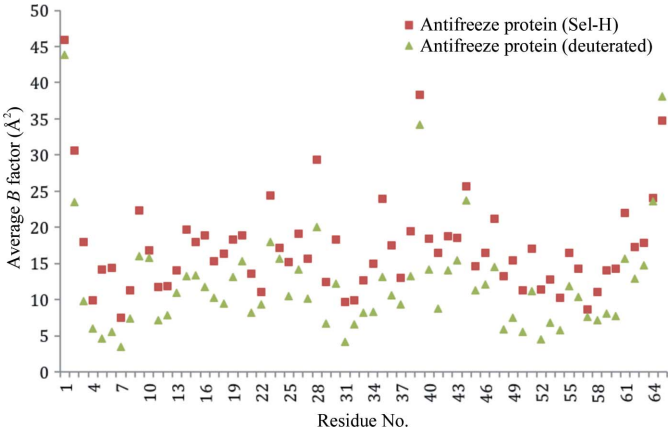

Figure 4
Comparison of average *B* factors for each residue between perdeuterated and selectively protonated deuterated type III antifreeze protein. The average difference in *B* factors between residues in the structures is 5.1 Å^2

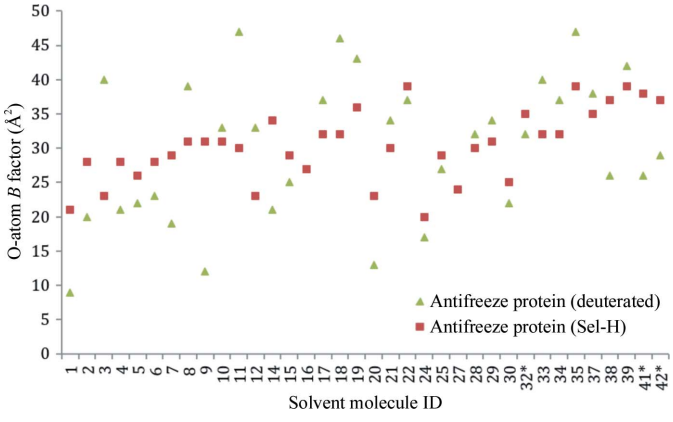

Figure 5
Comparison of solvent structure in the perdeuterated and selectively protonated deuterated neutron structures of type III antifreeze protein. 32 of the 42 molecules are in the same locations, with three in nearby positions (marked with asterisks). The average difference in *B* factors between solvent molecules in the structure is 7 Å^2.

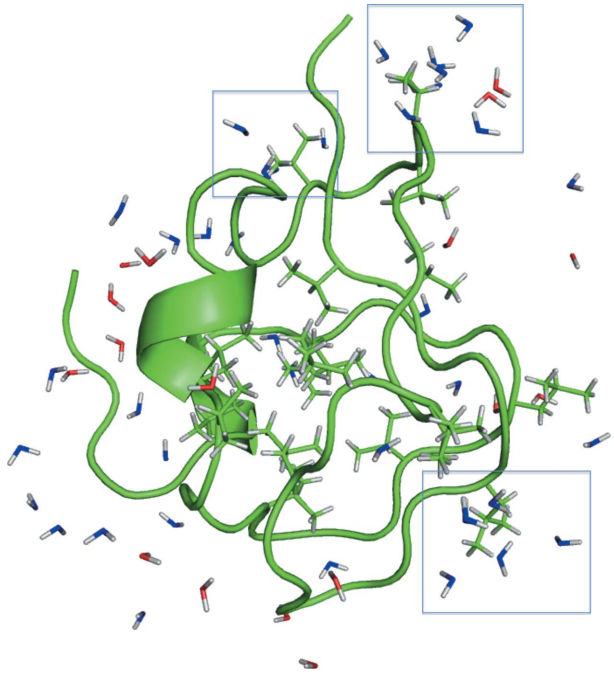

Figure 6
Differences in solvent structure between the perdeuterated (blue) and selectively protonated deuterated (red) structures. Solvent molecules found in the same positions have been omitted. Highlighted regions show the presence of water molecules in the perdeuterated structure but not in the selectively protonated deuterated structure which are in close proximity to the H atoms of valine or leucine residues.

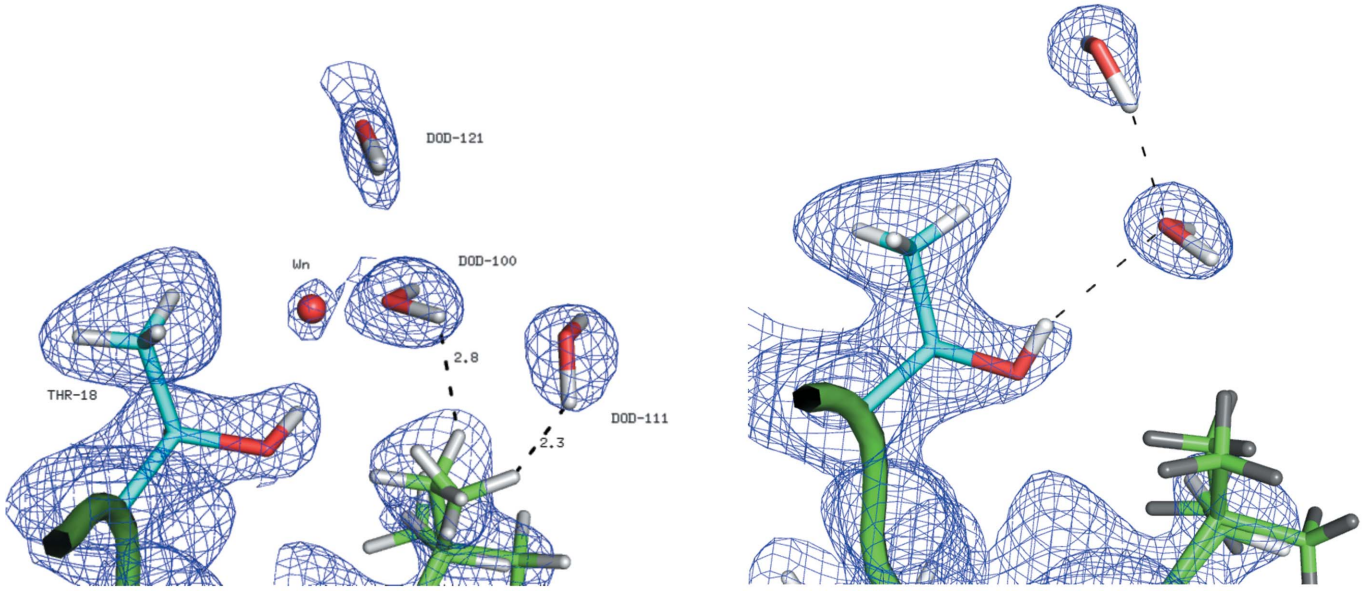

Figure 7
Tetrahedral water cluster in (*a*) perdeuterated (reproduced from Howard *et al.*, 2011, with permission) and (*b*) selectively protonated deuterated type III antifreeze protein. The $2F_o - F_c$ nuclear scattering density map is shown in blue contoured at 1 r.m.s.. D atoms are shown in white and H atoms in grey.

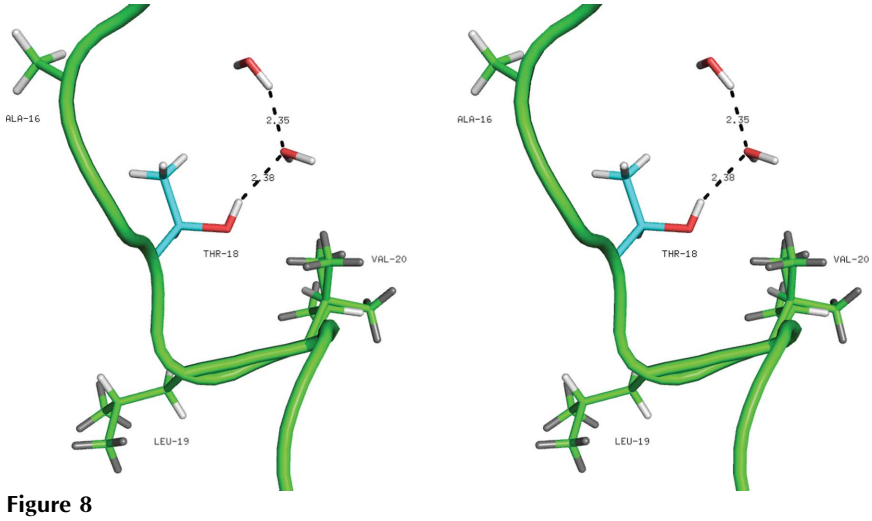

Figure 8
Stereoview (cross-eye) of Thr18, surrounding residues and the location of the expected tetrahedral water cluster. Val20 is methyl-protonated. D atoms are shown in white and H atoms in grey.

to the close proximity of Val20, which is methyl-protonated and hence produces negative scattering peaks that can cancel out the positive scattering peaks from the adjacent water molecules, reducing their visibility.

Fig. 7 shows a comparison between the selectively protonated deuterated and perdeuterated neutron structures with nuclear scattering density maps for Thr18 and the associated tetrahedral water molecules. Val20 is methyl-protonated, as well as being in a split conformation. Fig. 8 shows the region around Thr18 and the location of the expected tetrahedral water cluster along with adjacent residues for the selectively protonated deuterated structure.

4. Conclusions

The determination of the selectively protonated deuterated neutron structure of type III AFP has provided us with the opportunity to investigate cancellation effects involving H atoms by comparison with the perdeuterated neutron structure. A neutron structure obtained from a D_2O-soaked crystal (in which only labile H atoms are replaced by D atoms) would not have been as useful for this comparison, as the signal-to-noise ratio and hence the resolution limit would have been very different from those of the perdeuterated diffraction data (Blakeley *et al.*, 2008).

The selectively protonated leucine and valine residues do not appear to have affected the overall protein structure significantly. However, there were clear differences in the observation of water molecules between the selectively protonated deuterated and perdeuterated neutron structures, which are likely to arise from cancellation effects owing to the negative scattering from H atoms in the methyl groups of the protonated valine and leucine residues. This is particularly well illustrated in the case of the tetrahedral water cluster identified in the perdeuterated structure (Howard *et al.*, 2011). Only two of these four tetrahedral waters are visible in the selectively protonated deuterated neutron structure, and therefore this structure does not provide the information required to model the AFP–ice interaction. We therefore suggest that perdeuteration can be important in order to fully visualize water molecules in the

close vicinity of hydrophobic residues, as even a small number of H atoms are capable of obscuring the signal from adjacent water molecules.

SJF was supported by FWF grant P22862 from the Austrian Science Fund. All figures were prepared with *PyMOL* (DeLano, 2002). This work was supported by the Human Frontiers Science Program grant RGP0021/2006-C and benefited from the activities of the DLAB consortium funded by the European Union under contract HPRI-2001-50065 and from United Kingdom Engineering and Physical Sciences Research Council (EPSRC)-funded activity within the ILL Deuteration Laboratory under grant GR/R99393/01. We thank the ILL for provision of neutron beamtime on the LADI-III instrument. EIH is a member of the 'Carrera del Investigador', CONICET, Argentina. This work was supported by the Centre National de la Recherche Scientifique (CNRS), by the Institut National de la Santé et de la Recherche Médicale and the Hôpital Universitaire de Strasbourg (HUS).

References

Adams, P. D. *et al.* (2010). *Acta Cryst.* D**66**, 213–221.
Afonine, P. V., Mustyakimov, M., Grosse-Kunstleve, R. W., Moriarty, N. W., Langan, P. & Adams, P. D. (2010). *Acta Cryst.* D**66**, 1153–1163.
Arzt, S., Campbell, J. W., Harding, M. M., Hao, Q. & Helliwell, J. R. (1999). *J. Appl. Cryst.* **32**, 554–562.
Bhat, T. N. (1988). *J. Appl. Cryst.* **21**, 279–281.
Blakeley, M. P. (2009). *Crystallogr. Rev.* **15**, 157–218.
Blakeley, M. P., Kalb, A. J., Helliwell, J. R. & Myles, D. A. A. (2004). *Proc. Natl Acad. Sci. USA*, **101**, 16405–16410.
Blakeley, M. P., Ruiz, F., Cachau, R., Hazemann, I., Meilleur, F., Mitschler, A., Ginell, S., Afonine, P., Ventura, O. N., Cousido-Siah, A., Haertlein, M., Joachimiak, A., Myles, D. & Podjarny, A. (2008). *Proc. Natl Acad. Sci. USA*, **105**, 1844–1848.
Blakeley, M. P., Teixeira, S. C. M., Petit-Haertlein, I., Hazemann, I., Mitschler, A., Haertlein, M., Howard, E. & Podjarny, A. D. (2010). *Acta Cryst.* D**66**, 1198–1205.
Campbell, J. W., Hao, Q., Harding, M. M., Nguti, N. D. & Wilkinson, C. (1998). *J. Appl. Cryst.* **31**, 496–502.
Casadei, C. M., Gumiero, A., Metcalfe, C. L., Murphy, E. J., Basran, J., Concilio, M. G., Teixeira, S. C. M., Schrader, T. E., Fielding, A. J., Ostermann, A., Blakeley, M. P., Raven, E. L. & Moody, P. C. E. (2014). *Science*, **345**, 193–197.
Chen, J. C.-H., Hanson, B. L., Fisher, S. Z., Langan, P. & Kovalevsky, A. Y. (2012). *Proc. Natl Acad. Sci. USA*, **109**, 15301–15306.
Chen, V. B., Arendall, W. B., Headd, J. J., Keedy, D. A., Immormino, R. M., Kapral, G. J., Murray, L. W., Richardson, J. S. & Richardson, D. C. (2010). *Acta Cryst.* D**66**, 12–21.
Coates, L., Tomanicek, S., Schrader, T. E., Weiss, K. L., Ng, J. D., Jüttner, P. & Ostermann, A. (2014). *J. Appl. Cryst.* **47**, 1431–1434.
Cuypers, M. G., Mason, S. A., Blakeley, M. P., Mitchell, E. P., Haertlein, M. & Forsyth, V. T. (2013). *Angew. Chem. Int. Ed.* **52**, 1022–1025.
DeLano, W. L. (2002). *PyMOL*. http://www.pymol.org.
Emsley, P. & Cowtan, K. (2004). *Acta Cryst.* D**60**, 2126–2132.
Fisher, S. Z., Aggarwal, M., Kovalevsky, A. Y., Silverman, D. N. & McKenna, R. (2012). *J. Am. Chem. Soc.* **134**, 14726–14729.
Hazemann, I., Dauvergne, M. T., Blakeley, M. P., Meilleur, F., Haertlein, M., Van Dorsselaer, A., Mitschler, A., Myles, D. A. A. & Podjarny, A. (2005). *Acta Cryst.* D**61**, 1413–1417.
Howard, E. I., Blakeley, M. P., Haertlein, M., Petit-Haertlein, I., Mitschler, A., Fisher, S. J., Cousido-Siah, A., Salvay, A. G., Popov, A., Muller-Dieckmann, C., Petrova, T. & Podjarny, A. (2011). *J. Mol. Recognit.* **24**, 724–732.
Kovalevsky, A. Y., Hanson, B. L., Mason, S. A., Yoshida, T., Fisher, S. Z., Mustyakimov, M., Forsyth, V. T., Blakeley, M. P., Keen, D. A. & Langan, P. (2011). *Angew. Chem. Int. Ed.* **50**, 7520–7523.
Kurihara, K., Tanaka, I., Chatake, T., Adams, M. W. W., Jenney, F. E., Moiseeva, N., Bau, R. & Niimura, N. (2004). *Proc. Natl Acad. Sci. USA*, **101**, 11215–11220.
Munshi, P., Chung, S.-L., Blakeley, M. P., Weiss, K. L., Myles, D. A. A. & Meilleur, F. (2012). *Acta Cryst.* D**68**, 35–41.
Oksanen, E., Blakeley, M. P., El-Hajji, M., Ryde, U. & Budayova-Spano, M. (2014). *PLoS One*, **9**, e86651.
Ostermann, A., Tanaka, I., Engler, N., Niimura, N. & Parak, F. G. (2002). *Biophys. Chem.* **95**, 183–193.
Petit-Haertlein, I., Blakeley, M. P., Howard, E., Hazemann, I., Mitschler, A., Haertlein, M. & Podjarny, A. (2009). *Acta Cryst.* F**65**, 406–409.
Petit-Haertlein, I., Blakeley, M. P., Howard, E., Hazemann, I., Mitschler, A., Podjarny, A. & Haertlein, M. (2010). *Acta Cryst.* F**66**, 665–669.
Sanctis, D. de *et al.* (2012). *J. Synchrotron Rad.* **19**, 455–461.
Tomanicek, S. J., Blakeley, M. P., Cooper, J., Chen, Y., Afonine, P. V. & Coates, L. (2010). *J. Mol. Biol.* **396**, 1070–1080.
Weber, I. T., Waltman, M. J., Mustyakimov, M., Blakeley, M. P., Keen, D. A., Ghosh, A. K., Langan, P. & Kovalevsky, A. Y. (2013). *J. Med. Chem.* **56**, 5631–5635.
Weiss, K. L., Meilleur, F., Blakeley, M. P. & Myles, D. A. A. (2008). *Acta Cryst.* F**64**, 537–540.
Winn, M. D. *et al.* (2011). *Acta Cryst.* D**67**, 235–242.
Yokoyama, T., Mizuguchi, M., Nabeshima, Y., Kusaka, K., Yamada, T., Hosoya, T., Ohhara, T., Kurihara, K., Tanaka, I. & Niimura, N. (2013). *J. Synchrotron Rad.* **20**, 834–837.